INTERNATIONAL JOURNAL OF PURE AND APPLIED RESEARCH IN ENGINEERING AND TECHNOLOGY

A PATH FOR HORIZING YOUR INNOVATIVE WORK

INFLUENCE OF LANTHANUM DOPING ON STRUCTURAL, OPTICAL AND GAS SENSING PROPERTIES OF TIN OXIDE NANORODES

SACHIN T. BAHADE[1], AMRUT S. LANJE[1], SATISH J. SHARMA[2] AND AMRESH I. PRASAD[3]

1. Department of Electronics, Dr. Ambedkar College, Chandrapur (M.S.), India
2. Department of Electronics, R. T. M Nagpur University, Nagpur (M.S.), India
3. Department of Nanotechnology, North Eastern Hill University, Shilong, Meghalaya, India

Accepted Date: 30/10/2017; Published Date: 01/11/2017

Abstract: - In this paper, the synthesis of Lanthanum doped SnO_2 nanopawder (La:SnO_2) has been introduced by sol gel method using non-alkoxide $SnCl_4.2H_2O$, $C_6H_9LaO_6.aq$ as a precursors. The structural, optical and Gas sensing properties of the prepared La:SnO_2 powder sample has been carried out as a function of annealing temperature. The X-ray Diffraction (XRD), shows the samples have a tetragonal rutile structure with single phase. The Transmission Electron Microscopy (TEM) shows the average particle size is of ~6 nm for wt. at 8 %. Uv-vis spectra show low absorption at higher wavelength and strongest absorption at lower wavelength. PL spectra exhibits broad emission at 200 to 250 and emission peak at 220 nm.

Spin coated thin film for ethanol gas sensitivity increases with an increase in the operating temperature, reaching maximum value corresponding to 250 ^{0}C for all pure and doped sensors.

Keywords: Sol gel, La:SnO_2, Optical, Gas sensing

Corresponding Author: MR. SACHIN T. BAHADE

Access Online On:

www.ijpret.com

How to Cite This Article:

Sachin T. Bahade, IJPRET, 2017; Volume 6 (3): 1-18

PAPER-QR CODE

INTRODUCTION

In recent years, Tin oxides a sort of n-type semiconductor material have attracted a lot of interest due to their fascinating features, i.e high surface-to-volume ratio [1], strong carrier confinement [2], enhanced surface modes in their Raman spectra [3], and high transmittance and electrical conductivity [4]. These properties leads to applications in catalysis, gas sensing, and optoelectronics such as light emitting diode, Solar cells and panel displays [5-7] etc. Though a considerable effort has been given to obtain stoichiometric pure and La doped SnO_2 nanorodes at different concentration. The structural, optoelectronic and gas sensing properties have been investigated. The applied synthesis procedures have seen to affect substantially the crystallinity, microstructure and defect structure of the nanorodes. Several methods including sol-gel [8-9], hydrothermal [10], electrospinning [11] have been utilized to synthesize SnO_2. Among these techniques, the sol gel method seems suitable due to its simplicity, easy to add doping materials, promising for mass production and low cost. The properties of doped SnO_2 were found to be dependent on the processing conditions and nature of precursors used. The precursors play an important role in growth, the structure and the morphology as well as optical and electrical characteristics of the doped material. For optical devices like Solar cells, panel displays applications mainly affected by signal loss and delay; we have to improve the conductivity without affecting the transmission. Indeed, to improve and control the conducting properties of SnO_2 for wider range of possible applications, various elements such as Co [12], Sb[13], Mo[14], Li[15] and Nd[16] have been tested as doping. Similarly, Tin oxide play an important role for applications in Solar photo-thermal conversion [14, 17]. Recently, the rare earth doped semiconductor materials like La, Er, Ce, Yb have attracted much attention because of their applications in Optoelectronic devices [18]. Due to the limitation of solubility, these ions acts as grain growth inhibitors and remain aggregates at the grain boundaries. Although, to date there is few work has been carried out to investigate optical properties using La doped SnO_2. In the present work, sol gel synthesis method employed to obtain pure and La doped Nanorods and Nanoparticles at 500^0C. The effect of pure and with Lanthanum doped tin oxide is on crystallographic, Morphological, Optical and Gas sensing characteristics is studied. The obtained results are compared and discussed with several researchers.

2. MATERIALS AND METHODS:

2.1 Synthesis:

Nanocrystalline La doped SnO_2 samples were prepared by a Sol gel rout using Sn and La precursors taken in the form of chlorides and acetate respectively. In a typical synthesis process

of Pure and doped SnO_2, dissolve 5g of $SnCl_4$. $2H_2O$ from merck, India in 100 ml ethanol solution (Ethanol+ Water 1:1) and Stirred about 20 min until a transparent sol is produced. In order to investigate the effect of La dopant on structural and Optical properties, Lanthanium Acetate $C_6H_9LaO_6$.aq from Burgoyne Burbidge's & Co. Mumbai (India) was Added to the solution and stirred for 30 min. at different concentration 0 %, 2%, 5%, 8%, 15%. Add aqueous Ammonia solution (25% merck, India) drop wise to the solution under constant stirring and PH of solution was adjusted to a value up to 8. After 24 Hr of aging in the air resulting opal gel were centrifuged and washed with Ethanol at least 5 times to remove ammonia, chloride, acetate impurity. The collected gel was dried in furnace over 80^0C/4h in the air to remove moisture. Then after crush the sample and sintered at 500^0C/4 Hr. Finally ashed coloured nanoparticle powders were formed [8, 19-20]. Fabrication of thin film for sensor based on the material is done by spin coating method on 18mm x 18 mm glass plate at 4000 rpm, 40 sec and dry at 100^0C for 1h, and then it was preheated at 350^0C for 2 h and sintered at 500^0C for 2h in air.

2.2 Characterization techniques

First, the synthesized nanoparticles were Characterized by X-ray diffraction (XRD) measurements using a Bruker D8 Advance diffractometer with monochromatic CuK_α radiation (λ=1.5406 A^0) by recording θ in the range of 20-70^0 in a step of 0.02^0. To study the surface morphology & grain sizes, Scanning Electron microscopy(SEM) JEOL JSM 5600 with Resolution : 3.5 nm, Magnification : x18 to 300,000, Accelerating Voltage : 0.5 to 30 kV and Transmission electron microscopy (TEM) model JEOL/JEM 2100 was employed with acceleration voltage 200kV And 2000X – 1500000X magnification. ImageJ computer program were used to investigate the particle size distributions. Fourier Transform infrared (FT-IR) spectra of the powders were recorded using a Bruker, Germany, Model vertex 70 using the KBr pellet technique in the range 400 to 4000 cm^{-1} with a resolution of 0.5 cm^{-1}. Photoluminescence (PL) studies of prepared samples were carried out using a F-4500 FL spectrometer with 150 W Xenon lamp at room temperature. UV-Vis measurement was recorded using Jasco Spectrophotometer V-770 in a 200-1000 wavelength domain.

Finally, ethanol gas sensing measurement is carried out using gas sensing chamber, the change in resistance of sensors were recorded by USB digital multimeter on computer.

The sensor sensitivity is defined as S = Ra/Rg, Where Ra is the resistance in ambient air and Rg is the resistance in tested gas. Similarly, ethanol gas response time and recovery time were also recorded.

3. RESULT AND DISCUSSION

3.1 Structural investigation

XRD

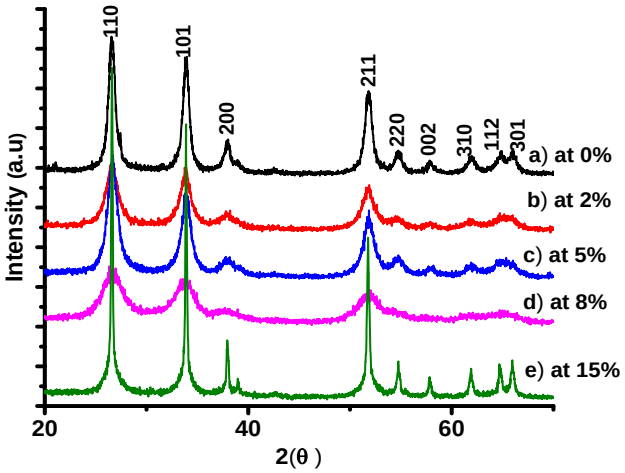

Figure 1: XRD pattern of La doped SnO_2.

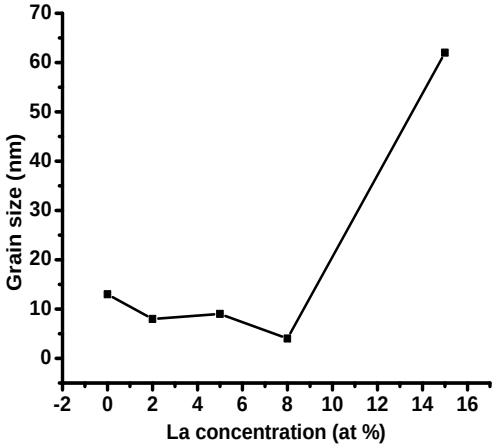

Figure 2: Variation of the grain size.

Table 1: XRD Data of La doped SnO_2 Samples and Pristine SnO_2 sample

Sample name	Crystalline size(nm)	a (A^0)	c (A^0)	a/c	Cell volume ($A^{0\,3}$) a^2c
Pure SnO_2	12	4.7401	3.1846	1.488	71.5553
La: SnO_2 at 2%	8	4.73627	3.1816	1.488	71.3718
La: SnO_2 at 5%	9	4.73469	3.1656	1.495	70.9659
La: SnO_2 at 8%	4	4.76362	3.1616	1.506	71.7443
La:SnO_2 at 15%	62	4.73820	3.1888	1.485	71.5907

To study the crystallite size, crystal structure and lattice parameters of La doped SnO_2, XRD analysis was used. The X-ray diffraction patterns of pure and lanthanum doped SnO_2 nanoparticles with various concentration sintered at 500^0C shown in Fig.1. The peaks were indexed using Powder X software and they are matched with the tetragonal rutile structure of SnO_2, which are consistent with the values in the standard card (JCPDS 77-0452) with a maximum intensity corresponding to (110) plane [21]. No impurity phase was observed in any

of the samples. There is no shift in the XRD peaks of the samples sintered at 500^0C and at different concentration indicating no change in the rutile structure with different concentration. Also, there are no peaks related to La content in these XRD patterns observed. The result shows that the intensity of peaks has been narrowed significantly, as the Lanthanum concentration increases (2%, 5%, 8%), but at 15% Lanthanum concentration intensity increases and all peaks showing clearly. Further it has been observed that lattice parameters a and c are calculated using unit cell software program and cell volume as shown in (Table 1). All calculated values are in good agreement with the reported values (JCPDS 77-0452). It can be seen that an increase or decrease of the lattice parameters "a" and unit cell volume, related to doping concentration in SnO_2. It may be attributed to the difference between ionic radius of Sn and La [22], which leads to stress in the host lattice and affect the crystalline nature of the material. The secondary phase cannot be observed may be due to La content dispersed uniformly in SnO_2. There are two possible mechanisms involved in the narrowing/broadening of the peaks; one is the particle size effect and other is lattice strain. In available literature we found that, some authors reported successful insertion La ion in the oxide lattice, while others are reported that La ions cannot be incorporated into crystals [23,24]. So, it strongly depends on preparation technique and doping concentration.

The average size of the crystalline grains of the sample was calculated using at full width half-maximum(FWHM) and Debye-Scherer's formula[25] given by :

$$D_{hkl} = \frac{0.9\lambda}{\beta\cos\theta}$$

Here, D_{hkl} is the crystalline size, λ is the X-ray wave length, β is the (110) full width at half maximum (FWHM) and θ is the angle of diffraction. The estimated sizes at the most intense crystallographic plane (110) are given in Table 1. The crystallite size of the pure and La doped SnO_2 nanoparticles are laying between 4-62 nm. We can see that when doping concentration upto 8 at %, this parameter decreases with doping, which is visible through a decrease in intensity of (110) peak, (Fig.1). However, the La concentration reach 15 at %, the crystallite size increases drastically up to 62 nm as well as the (110) peak intensity. The internal stress, strain, lattice distortion or defects can also affect the XRD peaks along with particle sizec[26]. When the doping level reached 15 at % La covers the surface of SnO_2 nanoparticles. This shows the limited solid solubility of Lanthanum in SnO_2. It contributes two effects First, to decrease of surface energy and lower the driving force [27]. The second, Tin oxide nanoparticles segregate from each other before the particles have grown into bigger size. Therefore, the thermal stability of the doped system can be improved and its boundary motion will be suppressed [13]. This increases the crystallite size of the sample 15 at % compared to others. The authors found

that the oxides like TiO_2, ZnO, CuO can disperse on to the surface of Tin Oxide causing a decrease in crystallite size. The incorporation of La into Tin oxide by the formation of Sn-O-La bond on the surface of small particles. This increases the stabilization of the small particles and confirming the role of La as a grain growth inhibitor [28]. The ratio of the lattice parameters a and c is a measure of lattice distortion, it has been calculated from XRD data (Table 1). The a/c ratio appears as constant in all the samples which that the lattice distortion is independent of lanthanum concentration in our samples. This suggests that all the atomic layers are equally strained at any lanthanum concentration. From the above discussion, it can be concluded that the narrowing or broadening of the XRD peaks of SnO_2 nonoparticles occurred due to atomic diffusion and lattice strains and not by lattice distortions. The particle size calculated by Scherer formula for La:SnO_2 5 at % have been further validated by Transmission Electron Microscopy(TEM) observations. Increase in Unit cell volume shows expansive strain in the particles and decrease in unit cell volume shows compressive strain in the particles.

3.2 SEM/TEM

Fig.3 shows the typical morphology and composition of pure and La:SnO_2 nanopowder at wt 2 %, 5 %, 8 %, 15 %. Powder samples were used for SEM analysis. Powder was stick on the sample holder using double sided tape and gold coated with sputter coater. It is seen that SEM image of Lanthanum doped SnO_2 at wt. 2 % and 8 %, microstructure of these powder samples shows the presence of large spherical aggregates of smaller individual nanoparticles with variations in particles size.

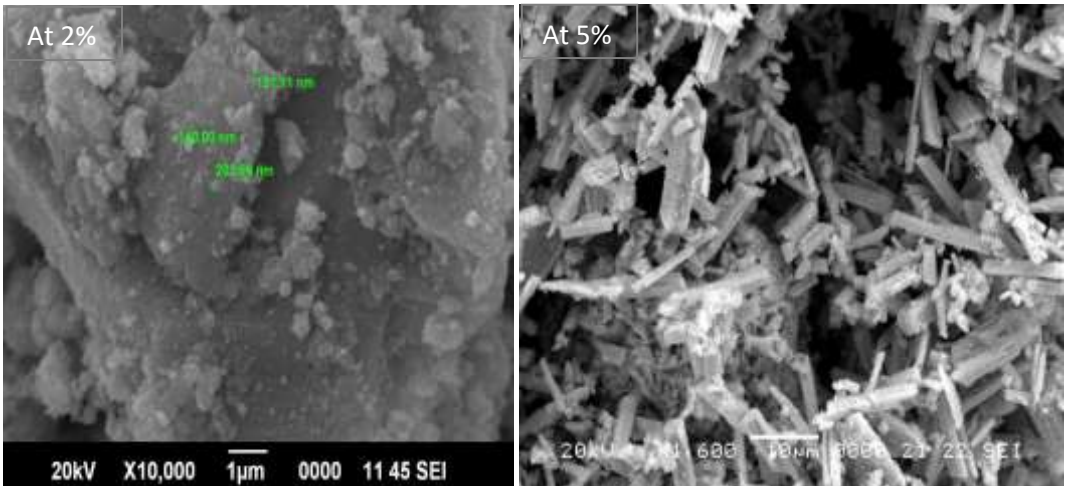

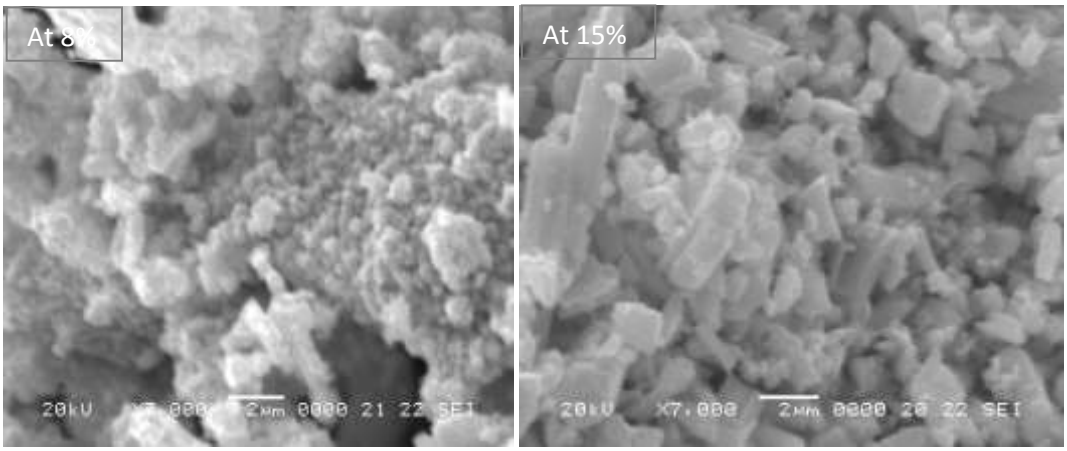

Figure.3 : SEM image of La:SnO_2 at 2 %, 5 %, 8 %, 15 %

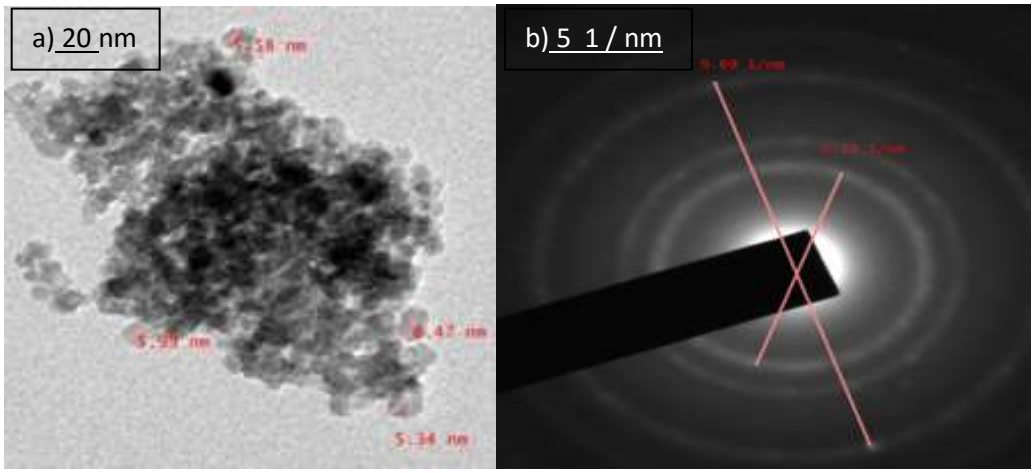

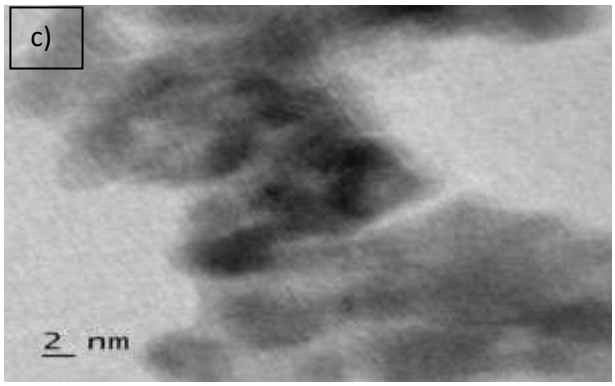

Figure 4: Shows TEM image of prepared Lanthanum doped SnO_2 at wt. 8 % .

For wt. at 5 % & 15 % are looking like nanorods. Due to the large surface and high surface energy of primary nanoparticles, Tin Oxide tiny particles are prone to aggregated [29]. The enhancement of grain size with doping level confirms the presence of La ions 15 at % into SnO_2 crystal which bothers the particle growth. The randomly grown grains gives rise in scattering effect, which reduces the transmittance [30]. The surface state of such oxide nanoparticles influence there optical and electrical properties which are essential to ensure the implementation of the different optoelectronic devices and gas sensors.

Fig.4 Shows TEM image of prepared Lanthanum doped SnO_2 nanoparticles at 8 % showing an average diameter of about ~6 nm as well. For this powder samples were dispersed in ethanol and sonicated in an ultrasonic bath. The particle size obtained from TEM analysis is slightly higher than the crystalline size calculated from XRD data.

3.3 FT-IR

FT-IR spectra were recorded in solid phase by using KBr pellets technique in the region of 400-4500 cm^{-1}. FT-IR spectra of pure and Lanthanum doped SnO_2 nanoparticles at 0 %, 2 %, 5 %, 8 %, 15 % prepared at 500 ^0C are shown in Fig. 5, and it is clear from the figure that there are clear changes in the shapes and positions of IR peaks indicating that La might have been incorporated in SnO_2 host. The observed frequency at 450 cm^{-1} is assigned to the symmetric Sn-O-Sn stretching mode. Antisymmetric Sn-O-Sn stretching mode of the surface hydroxyl groups is obtained at 650 cm^{-1} is observed. The broad band between 500 to 800 cm^{-1} due to the vibrations of Sn-O-Sn mode of tin oxide [8, 31-32]. It is clear from the figure that the all the vibration broadens with the increase in doping concentration. This might be reducing the particle size with doping concentration. Secondly, the broadening can also be attributed to the defects generated in the system. The peak at 1000 cm^{-1} is related to the vibration of hydroxyl-tin (Sn-OH) bond. The vibrations from 1300-1600 cm^{-1} is assigned to the C-O stretching mode [33-34]. The bands appearing in all the samples around 1650 cm^{-1} might be due to the bending mode of O-H bonds. Lastly, the broad band appearing in the region 2500-3500 cm^{-1} may be due to vibration of adsorbed water. The present assignments corroborate well with the values very near to the reported available literature [35-37].

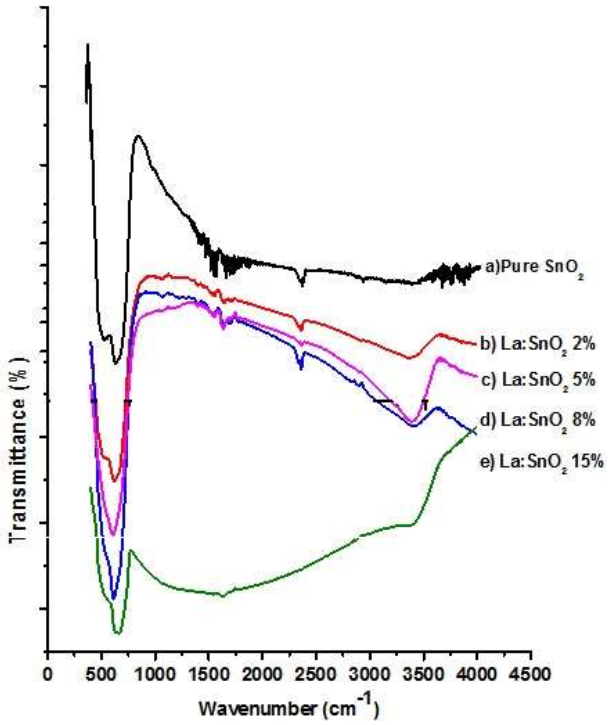

Figure 5: FT-IR graph of La:SnO_2 at 2% ,5%,8%,15%

3.4 Photoluminescence study

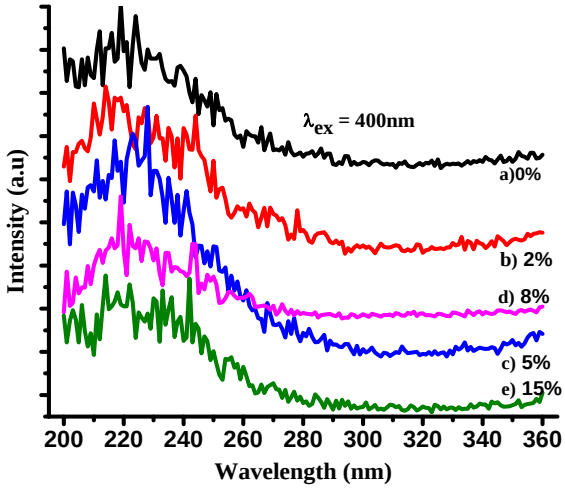

Figure 6: Room temperature photoluminescence emission spectra (at λ_{ex} = 400 nm) for pure and La doped SnO_2 samples.

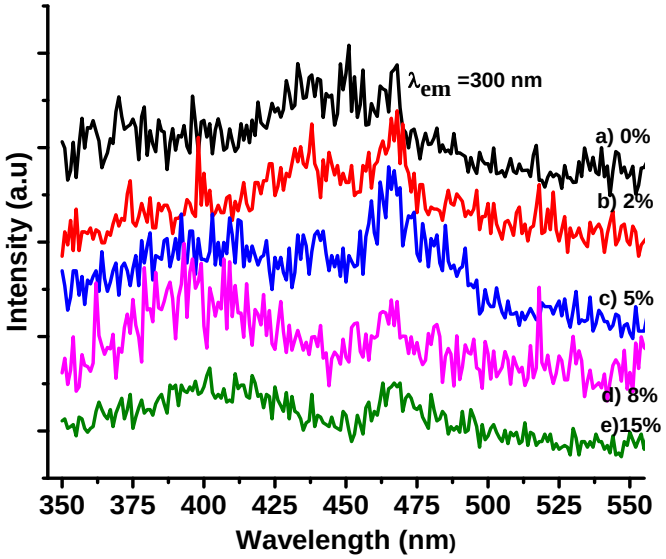

Figure 7: Room temperature Photoluminescence excitation spectra (at λem = 300 nm) for pure and La doped SnO_2 samples.

The room temperature Photoluminescence behavior of pure and La doped SnO_2 nanoparticles was investigated using PL spectrometer. Fig.6 contains the photo induced fluorescence spectra of all samples for an excitation wavelength 400 nm. It can be seen from the PL spectra the samples exhibit broad emission at 200 to 250 and one emission peak at 220 nm.

This emission bands presents due to essentially to the presence of point defects, such as oxygen vacancies in SnO_2 nanoparticles [38-39]. It can be seen from the Fig 6. That there is slightly shift the PL peak position before or after the 220 nm as doping concentration increases. However, a slight increase in the intensity of luminescent emission was observed with doping which can be attributed to the defects such as oxygen interstitials and La vacancies in the doped samples.

Fig 7 shows room temperature PL excitation spectra (at λem = 300 nm) for nano crystalline and Nano rode La doped SnO_2 samples at 0 %, 2 %, 5 %, 8 %, 15 % respectively. The 2 broad excitation bands are observed at 350-450 and 450-500 nm at constant emission 300nm. The major peaks are observed of pure SnO_2 at 350 to 450nm band with very poor intensity, but at 450-500 nm the highest peaks observed are 405 nm and 470nm. For 2 % concentration highest peaks observed at 400nm, 463nm and 470nm and other peaks are at lower intensities. Peaks observed at 470nm is common in all samples with decrease intensities at 8% and 15% La:SnO_2.

3.5 UV-Vis

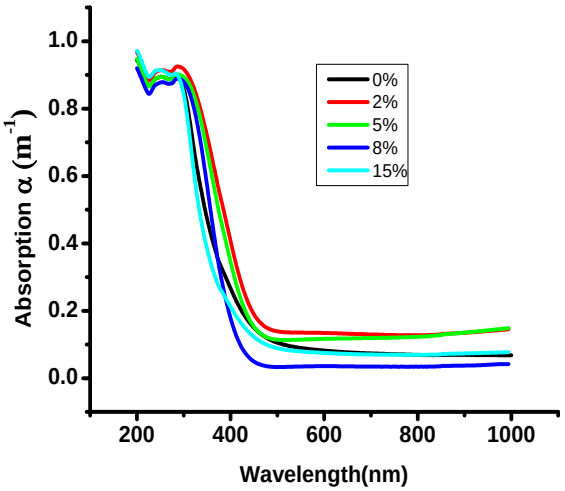

Figure 8: The absorption coefficient α(λ) of La:SnO_2

Fig.8 shows the absorption coefficient α(λ) of La doped SnO_2 nanoparticles from 200 to 1000 nm range. All samples showing low absorption at higher wavelength and strongest absorption at lower wavelength. The absorption spectra between 200 to 450 nm, shows a maximum around 200 and 300 nm, which indicates the photo-excitation of electrons from the valence band to the conduction band. It is well established that the absorption depends on several factors such as crystalline size, surface roughness, defect density etc. Hence, only the structural study did not reveal significant changes in the morphology of the samples. For that we have to increase of the absorption to increase of the density of the defects and disorder, which are very related to the to the reduction of crystallite size. Indeed, an increase in dislocation density values and microstrain gives rise to crystal defects and disorders in Tin oxide lattice [30]. Thus, with more defects, the electronic transitions from the filled valence band to the energy level of defects.

On the other hand, In order to calculate the optical band gap (Eg) we used the Tauc's relation,

$$\alpha h\nu = A'(h\nu - Eg)^n$$

Where, α is the absorption coefficient, A is a constant while the exponent n depends on the type of transition (n=2 for indirect allowed, n=1/2 for direct band gap semiconductor). Therefore, the optical band gap is obtained by extrapolation of the linear region of a tauc's plot

by plotting $(\alpha h\nu)^2$ vs $h\nu$. The Tauc's plot of Pure and La doped samples are shown in Fig.9 with inset showing the obtained values of the band gaps. The measured band gap Eg was found to be in the range of 2.7 to 3.3 eV, which is slightly small to the reported values of bulk SnO_2 i.e 3.6 eV [40]. It can be seen that the band gap values shows increase or decrease tendency with La doping content in Tin oxide structures. This can be attributed due to quantum confinement effect [41], reorientation effect [42], microstrain and dislocation density in nanoparticles. Thus, many researchers reported that, with higher level of defects, the electronic transitions occurs from the filled valence band to the energy levels of defects instead of the filled valence band to empty conduction band. These phenomena leads to band tail and shrinkage of the band gag i.e Burstein Moss shift [43].

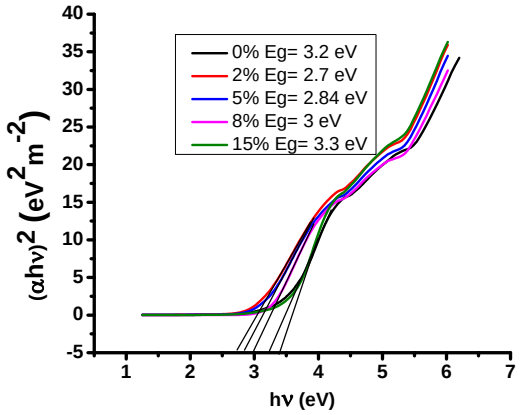

Figure 9: Tauc Plot of $(\alpha h\nu)^2$ vs $h\nu$

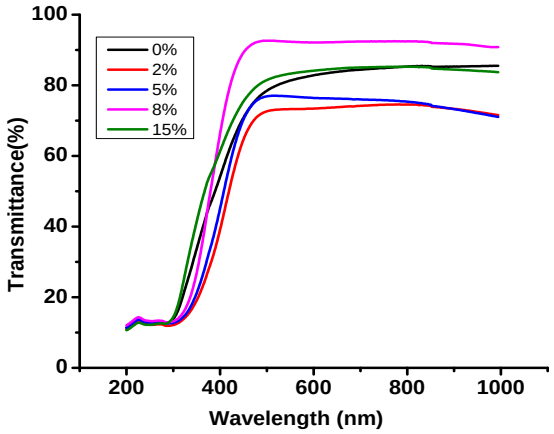

Figure 10: The Transmittance coefficient of La:SnO_2

Fig.10, shows the optical transmittance spectra of La doped nanoparticles in the wavelength region 200 – 1000 nm. These spectra show that the prepared nanoparticles exhibit a transparency coefficient lying between 65 to 95 % in the visible range. Further, it is observed that transmittance shows decreasing or increasing tendency with doping concentration. Which is related to the change of light scattering, crystalline size and free carrier absorption of photon. It is also reported that high carrier concentration increases IR diffusion, which leads to a reduction of transmittance.

3.6 GAS SENSING PROPERTIES

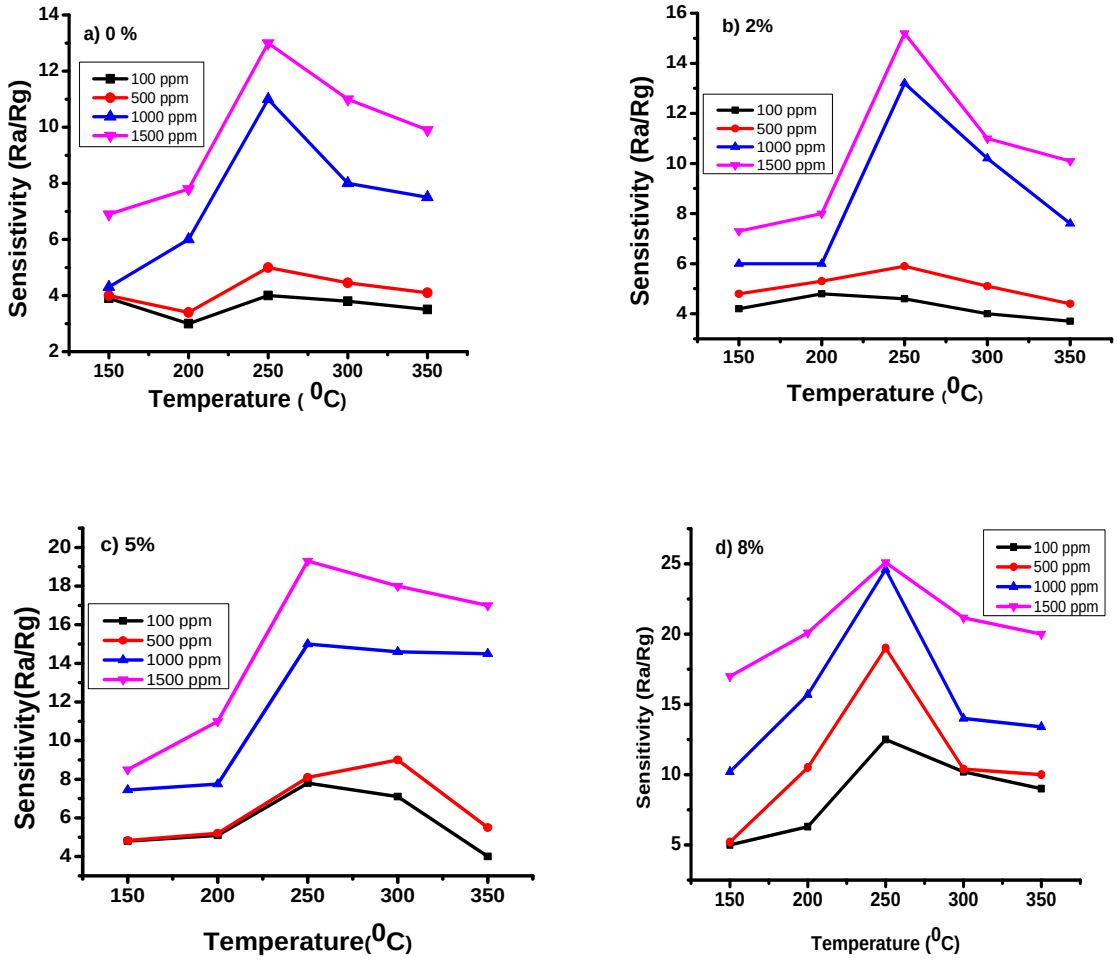

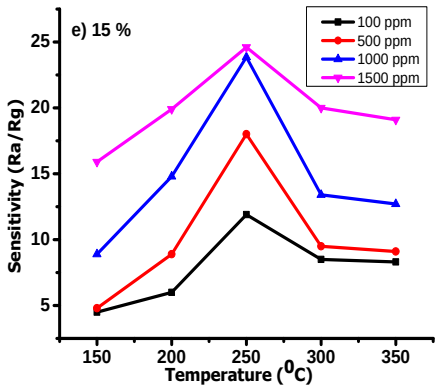

Figure 11: Ethanol gas sensitivity a) 0% b) 2% c) 5% d) 8% e) 15%

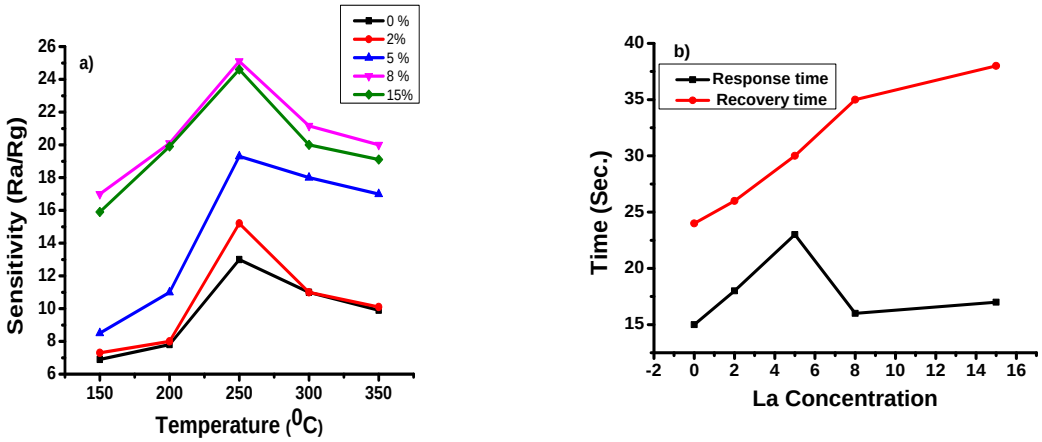

Figure 12 a) Sensitivity variation b) Response and recovery time of pure and La doped ethanol sensors towards 1500 ppm at 250^{0}C.

The Gas sensitivity of pure and La doped tin oxide as a function of operating temperature range 150 to 350^{0}C and Ethanol gas concentration (100 -1500 ppm) is displayed in Fig. 11a-e. Fig. 12 shows sensitivity variation of 0%, 2%, 5%, 8%, 15% La dope tin oxide sensor at 150-350^{0}C towards 1500 ppm of ethanol gas. It is observed that highest sensitivity is achieved under exposure to 1500 ppm of ethanol gas at 250^{0}C for all the pure and doped tin Oxide sensors. For undoped sensor, the highest sensitivity is 13 whereas for 2%, 5%, 8%, 15% La doped tin oxide sensor, highest sensitivity are 15.5, 19.5, 25.6 and 24.8 respectively.

From Fig. 11-12, it concludes that sensitivity increases with an increase in the operating temperature, reaching maximum value corresponding to 250^{0}C for all pure and doped sensors. However, further increasing the temperature above 250^{0}C ethanol sensitivity start to decrease

again. The optimum sensitivity can be attributed due to thermal energy obtained was high enough to overcome the activation energy barrier of the reaction, while reducing gas sensitivity was due to the difficulty in exothermic gas adsorption [44]. From the Figures it is evident that Lanthanum increases the ethanol sensitivity, and highest sensitivity observed at 8% La:SnO_2, then after sensitivity reduced at 15 wt. %.

Response and Recovery time: The response time is, the time taken by the sensor element to achieve 90% of stable output when the gas was introduced. The recovery time is, the time taken by the sensor element to reach 90% of its original value. Fig. 13 shows the response and recovery time of pure and La doped SnO_2sensor at 250^0C and 1500 ppm ethanol gas. It is observed that when the target gas was inserted in the gas sensing chamber the resistance of the sensor decrease drastically. However, when air was introduced resistance regains its original value. The time measured between response and recovery is shown details in Fig. 13.

It is observed that Pure sensor gives highest response and recovery time, But it increases when La concentration increases. The slower response time indicates the decrease of chemical composition. Besides, the response and recovery time is affected due to activation energy of chemical reaction. In order to decrease response and recovery time of tin oxide based sensor other noble metals may reduce the activation energy of chemical reaction.

4. CONCLUSION AND OUTLOOK

This paper deals with some structural, optical, gas sensing characterization of obtained nanoparticles by sol gel method at 500^0C. The XRD study shows that the obtained powder have rutile tetragonal structure. Upon increasing the La doping concentration the crystalline quality was found to be affected. SEM images reveal the presence of agglomerates and a reduction in grain size rode shaped with La content. TEM image 8 at % confirms that its size closely matches with XRD value.

Second, The IR Spectra shows that all the vibration broadens with the increase in doping concentration. PL emission shows slight increase in the intensity was observed with doping. Which contribute to the photocatalytic applications. UV-vis was investigated to study Absorption coefficient of doped material.

Finally, Ethanol gas Sensitivity, Response time and Recovery time was studied at different La doping concentration by spin coated sensors. The experimental result indicates that 8 at % La:SnO_2 sensor exhibited highest sensitivity at 250^0C temperature.

ACKNOWLEDGEMENT:

The author gratefully acknowledge the UGC-DAE Center, Indore for XRD, SEM, FTIR and DST-SAIF, kochi for TEM. We need to convey our thanks to Dr. R. S. Ningthoujam, Chemistry Division, BARC, Mumbai for PL measurement.

REFERENCES:

1. N. S. Baik, G. Sakai, K. Shimane, N. Miura, and N. Yamazoe, (200), Sens. Actuators B, 65 (1-3), 97-100.
2. E. J. H. Lee, C. Reibeiro, T. R. Giraldi, E. Longo and E. R. Leite, (2004), App. Phys. Lett., 84(10), 1745-1747.
3. J. Zuo, C. Xu, X. Liu, C. Wang, Y.Hu and Y. Qian , (1994), J.Appl.Phys., 75(3), 1836.
4. C. Marbet, A. Boukhachem, M. Amlouk, T. Manaubi, Journal of Alloys and compounds (2016).
5. M. Epifani, J. Arbio, E. Pellicer, E. Comini, P. Siciliano, G. Faglia and J. R. Morante, , Cryst. Growth Des. (2008), 8(5), 1774-1778.
6. L .H. Qian, K. Wanga, H. T. Fang, Y. Lia, and X .L. Maa, Mater. Chem. Phys. (2007),,103(1), 132-136.
7. H. Y. Yang, S. F. Yu, H. K. Liang, S. P. Lau, S. S. Pramana, C. Ferraris, C. W. Cheng, and H .J. Fan (2010), Appl. Mater. Interfaces, 2(4), 1191-1194.
8. A. S. Lanje, S. J. Sharma, R. B. Pode and R. S. Ningthoujam , Arch. Apll. Sci. Res., 2010, 2 (2):127-135.
9. S.Gnanam and V. Rajendran (2010), J. Sol-Gel Sci. Technol., 53(3),555-559.
10. H. T. Chen, X. L. Wu, Y. Y. Zhang, J. Zhu, Y. C. Cheng and P. K. Chu,(2009), Appl. Phys. A, 97 (3), 581-585.
11. Q. Qia, T. Zhanga, L. Liua and X. Zheng, (2009), Sens. Actuators B, 137(2), 471-475.
12. K. Srinivas, M. Vithal, B. Sreedhar, M. Manivel Raja and P. Venugopal Reddy, J. Phys. Chem. *C* 2009, Vol. 113 No. 9, 3543-3552.
13. G. T. Ang, G. H. Toh, M. Z. Abu Bakar, A. Z. Abdullah, M. R. Othman, Process Safety and Environmental Protection, 89 (3) (2011) 186.
14. G. Turgut, E. Sonmez, *Superlattices and Microstructures,* 69 (2014) 175.
15. D. Paul Joseph, P. Renuhambal, M. Saravanan, S. Philip Raja, C. Venkateshwaran, Thin Solid Films, 517 (2009) 6129.
16. G. Turgut, E. Sonmez, S. Duman, *Material Science in Semiconductor Processing,* 30 (2015) 233.
17. E. Elangovan, K. Ramamurthi, Journal of Optoelectronics and Advanced Materials, 5 (2003) 45.

18. R. Zamiri, A. F. Lemos, A. Reblo, H. A. Ahangar, J. M. F. Ferreira, Ceramics international, 40 (2014) 523.
19. K. Sriniwas, M. Vithal, B. Sreedhar, M. Raja & P. Reddy, J. Phys. Chem. C, Vol.133, No.9, 2009, 3543-3552.
20. A.M.EI-Sayed, S. M. Yakut, Journal of Research in Nanotechnology, Vol.2016(2016).
21. A. D. Mighell, C. R. Hubbard, J. K Stalick, M. A. Holomany, NBS AIDS83 JCPDS-International Centre for Diffraction Data, Swarthmore, *PA, U.S.A*, 1983.
22. R. D. Shannon, Acta Crystallographica Section A: Crystal Physics, Diffraction, Theoretical and General Crystallography, 32 (1976) 751.
23. J. Jia, F. Luo, C.Sau, X. Wang, H. Song, X. Hu, Ceramics International, 40 (2014) 6973.
24. L. P. Chikhale, J. Y. Patil, A.V. Rajguru, F. I. Shaikh, I. S. Mulla, S. S. Suryawanshi, Ceramics International, 40 (2014) 2179.
25. B. D. Cullity, Elements of X-ray Diffraction, (1978) A. W. Pub. Comp. Inc., Bostan.
26. I. Navas, R. Vinodkumar, K. J. Lethy, M. Satyanarayana, V. Ganeshan and V. P. Mahadevan Pillai, J.Nanoscience and Nanotechnology, 9 (2009).
27. A. P. Macial, P. N. Lisboa-Filho, E. R. Leite, C.O. Paiva-Santos, J. Eur. Ceram. Soc., 23 (2003) 707.
28. M. M. Maletin, R. R. Denadi, L. M. Nikoli, V. V. Srdi, J. Optoelectron. Adv. Mater., 9 (7) (2007) 2245.
29. L. Chao, W. Wei, X. Tanguchi, W. Huanxin, Z. Youqi, S. Yanliag, J. of Rare Earths, 28 (2010) 161.
30. F. Yakuphanouglu, Y. Caglar, S. Ilican, M. Caglar, Phys. B, 394 (2007) 86.
31. H. Frohlick, Theory of Dielectrics, Oxford University press (1956)
32. P. I. Archer, P. V. Radovanovic, S. M. Heald and D.R.Gamelin, J. Am. chem. Soc., 127, 14479(2005)
33. P. G. Horrison and A. J. Guest, J. Chem. Soc., Faraday Trans. 83 (1987) 3383.
34. Z. Jun-Jei, Z.Jian-Min, L. Xue-Hong, F. Jiang-Lin, Miao-Gaozhou and C. Hong-Yuan, Mat. Lett., 53 (2002) 12.
35. Jun-Jie Zhu, Jian-Min Zhu, X. Liao, J. Fang, M. Zhou, H. Chen, Mat. Lett., 53 (2003) 12.
36. K. Srinivas, M. Vithal, B. Sreedhar, M. M. Raja and P. V. Reddy, J. Phys. Chem. C, 113 (2009) 3543.
37. P. G. Harrison and A. Guest, J. Chem. Soc, Faraday Trans., 183 (1987) 3383.
38. S. Luo, J. Fan, W. Liu, M. Zhang Song, C. Lin, X. Wu and P. K. Chu, (2006) Nanotechnology, 17(6) 1695-1699.
39. R. Sánchez Zeferino la, U. Pal, R. Meléndrez and M. Barboza Flores, Advances in Nano Research, Vol. 1, No. 4 (2013) 193-202.

40. L. M. Fang, X. T. Zu, Z. J. Li, S. Zhu, C .M. Liu, L. M. Wang and F. Gao, J. Mater. Sci. Mater. Electron., 19 (2008) 868-874.
41. T. Takagahara and K. Takeda, Phys. Rev. B, 46 (1992) 15578-15581.
42. G. Turgut, E-F. Keskenler, Se. Aydin, E. Sonmez, S. Dogan, B. Duzgun, M. Ertugrul, Superlattices and Microstructures, 56 (2013) 107.
43. E. Burtein, Phy. Rev. 93 (1954) 632.
44. J. F. Chang, H. H. Kuo, I, C. Leu and M. H. Hon, Sensors Actuator B Chem.,84 (2002) 258-264.
45. A. S. Lanje, S. J. Sharma and R. S. Ningthoujam, IJPRET, 2013;Vol. 1(8): 54-63.
46. A. S. Lanje, R. S. Ningthoujam, S. J. Sharma and R. B. Pode, Indian Journal of Pure & App. Phy., Vol. 49, 2011, pp. 234-238.